were incubated with antibody PAb 122 (*15*) for 45 min at room temperature, washed in phosphate-buffered saline, incubated with a Cy3-coupled goat antibody to mouse immunoglobulin G (Dianova, Hamburg, Germany) for 30 min, washed, and photographed. Cells were then denatured by 2 N HCl for 15 min at room temperature, washed, and incubated with a fluorescein-coupled mouse antibody to BrdU (Boehringer). Finally, cells were incubated 5 min with bisbenzimide H 33258 (1 μg/ml) (Calbiochem, San Diego, CA) for chromatin staining. We determined the number of cells eliminated by apoptosis by counting cells within individual fields on the cover slip before, and 24 hours after, addition of β-estradiol. The determination was done with at least 2000 cells in four independent experiments for each cell line. The rate of DNA synthesis was evaluated as the ratio of BrdU-incorporating cells to viable cells 24 hours after addition of β-estradiol.

6. H. Hermeking and D. Eick, unpublished data.
7. Serum-starved LM-3 cells were lysed in Laemmli buffer at various time points after addition of β-estradiol. Identical amounts of proteins were separated on a 12.5% polyacrylamide gel, transferred onto a nitrocellulose membrane, and probed with antibody PAb 240, which recognizes both mutant and denatured wt p53 protein (*16*) (Ab-3, Dianova). Signals were generated with the enhanced chemiluminescence detection system (Amersham) with a horseradish peroxidase–coupled secondary antibody (Promega, Heidelberg, Germany). Immunoblot analysis was performed as described (*17*).
8. RNA was isolated, and identical amounts were separated on a 1% formaldehyde-agarose gel, transferred onto a nylon membrane (Hybond N+, Amersham), and hybridized with a ^{32}P-labeled murine p53 complementary DNA. The signals were measured with a PhosphoImager (Fuji). Northern (RNA) blot analysis was performed as described (*17*).
9. N. C. Reich and A. J. Levine, *Nature* **308**, 199 (1984).
10. M. B. Kastan, O. Onyekwere, D. Sidransky, B. Vogelstein, R. W. Craig, *Cancer Res.* **51**, 6304 (1991); M. B. Kastan *et al.*, *Cell* **71**, 587 (1992); X. Lu and D. P. Lane, *ibid.* **75**, 765 (1993).
11. H. Hermeking *et al.*, *Proc. Natl. Acad. Sci. U.S.A.*, in press.
12. L. A. Donehower *et al.*, *Nature* **356**, 215 (1992); M. Harvey *et al.*, *Oncogene* **8**, 2457 (1993).
13. S. W. Lowe, H. E. Ruley, T. Jacks, D. E. Housman, *Cell* **74**, 957 (1993); S. W. Lowe and H. E. Ruley, *Genes Dev.* **7**, 535 (1993); M. Debbas and E. White, *ibid.*, p. 546.
14. V. Kumar, S. Green, A. Staub, P. Chambon, *EMBO J.* **5**, 2231 (1986).
15. E. G. Gurney, R. O. Harrison, J. Fenno, *J. Virol.* **34**, 752 (1980).
16. J. V. Gannon, R. Greaves, R. Iggo, D. P. Lane, *EMBO J.* **9**, 1595 (1990).
17. J. Sambrook, E. F. Fritsch, T. Maniatis, *Molecular Cloning: A Laboratory Manual* (Cold Spring Harbor Laboratory Press, Cold Spring Harbor, NY, ed. 2, 1989).
18. We thank L. A. Donehower for p53$^{-/-}$ cells; M. Eilers for NIH 3T3.LTR-MycER cells; P. Chambon for ER-cDNA (HE-14); G. Brander for PAb 122; G. Greene for ER-specific antibody H222; B. Kempkes for expression plasmids and technical advice; C. Dalke for oligonucleotides used for sequence analysis; A. Pullner for perfect technical assistance; and members of our institute for discussion and critical reading of the manuscript. Supported by the Deutsche Forschungsgemeinschaft (SFB190; Mechanismen und Faktoren der Genaktivierung) and Fonds der Chemischen Industrie.

26 May 1994; accepted 26 August 1994

Premature Microtubule-Dependent Cytoplasmic Streaming in *cappuccino* and *spire* Mutant Oocytes

William E. Theurkauf

Embryonic axis specification in *Drosophila melanogaster* is achieved through the asymmetric subcellular localization of morphogenetic molecules within the oocyte. The *cappuccino* and *spire* loci are required for both posterior and dorsoventral patterning. Time-lapse confocal microscopic analyses of living egg chambers demonstrated that these mutations induce microtubule reorganization and the premature initiation of microtubule-dependent ooplasmic streaming. As a result, microtubule organization is altered and bulk ooplasm rapidly streams during the developmental stages in which morphogens are normally localized. These changes in oocyte cytoarchitecture and dynamics appear to disrupt axial patterning of the embryo.

The functional asymmetries that specify the axes of the *Drosophila* embryo are established during oogenesis stages 8 through 10 (*1*–*4*). During these stages, the oocyte nucleus moves to the dorsal surface (*5*); *bicoid* mRNA, the primary anterior morphogen, is localized to the anterior cortex (*6*); *oskar* mRNA and the proteins encoded by *staufen* and *vasa*, which are required for posterior patterning and pole cell formation, are positioned at the posterior pole (*3*, *4*, *7*–*9*); and *gurken* mRNA, which plays an essential role in dorsoventral axis specification, accumulates between the dorsally located oocyte nucleus and the cortex (*10*).

The microtubule cytoskeleton appears to play a key role in the establishment of axial asymmetry in *Drosophila* oocytes. Microtubule assembly inhibitors disrupt dorsal localization of the oocyte nucleus, anterior positioning of *bicoid* mRNA, and posterior accumulation of *oskar* mRNA and the protein encoded by *staufen* (*11*–*13*). Reorganization of the oocyte microtubule cytoskeleton is also temporally and morphologically correlated with the initiation of morphogen localization (*14*). During stages 8 through 10, microtubules associate preferentially with the anterior cortex of the oocyte, so that a broad anterior to posterior cortical gradient is present at stage 9. This distribution of cortical microtubules mirrors the initial transient anterior localization of *oskar* mRNA and the anterior distribution of *bicoid* mRNA (*14*). The microtubule cytoskeleton reorganizes a second time during stage 10b, when the transfer of nurse cell cytoplasm and ooplasmic streaming begins (*15*). At this time, the anteroposterior microtubule network is replaced by arrays of parallel microtubules that form adjacent to the oocyte cortex (*14*). Inhibitor studies indicate that ooplasmic streaming is microtubule-dependent and is likely to be driven by organelle transport along the subcortical microtubules (*14*, *15*).

Mutations at the *cappuccino* (*capu*) and *spire* (*spir*) loci alter both posterior and dorsoventral patterning, which raises the possibility that they affect the cytoskeletal functions that mediate axis specification (*16*). To determine if the *capu* and *spir* mutations influence axial polarization of the microtubule cytoskeleton, I injected living oocytes with rhodamine-conjugated tubulin and directly examined microtubules with laser scanning confocal microscopy (Fig. 1). Analysis of wild-type oocytes with this in vivo technique generally confirms the results of previous immunocytochemical studies (*14*). Oocytes from stages 8 through 10a contained a random network of cytoplasmic microtubules, with the highest density of microtubules associated with the anterior cortex (Fig. 1A). After initiation of ooplasmic streaming, during stage 10b, parallel arrays of microtubules could be observed just beneath the oocyte cortex (Fig. 1B). These subcortical microtubules persist through stage 12 and disassemble during stage 13, when streaming stops (*17*). The network of ooplasmic microtubules observed deep within living stage 8 through 10a oocytes was more extensive than that observed in fixed material. This difference may be the result of incomplete penetration of tubulin antibodies into the interior of the oocyte during immunolabeling (*14*).

The *capu* and *spir* mutations are identical in their effects on posterior and dorsoventral axis specification, which suggests that they define components of a single biochemical system (*16*). These mutations also produce similar changes in the organization of microtubules within the developing oocyte. Immunofluorescence analyses indicate that the *capu* and *spir* mutations do not affect microtubule organization during stages 2 through 6 (*17*). However, these mutations induce a change in the microtubule cytoskeleton during stages 8 through 10a. Early in stage 8, prominent sub-

Department of Biochemistry and Cell Biology, State University of New York, Stony Brook, NY 11794, USA.

cortical microtubule arrays were observed within mutant oocytes (Fig. 1C). These microtubule arrays persist through stage 12 and disassemble as the oocyte matures during stage 13 (*17*). The organization of microtubules in stage 8 through 10a *capu* and *spir* oocytes is similar to that of wild-type oocytes during ooplasmic streaming, which is normally restricted to stages 10b through 12. These observations suggested that the *capu* and *spir* mutations may affect the developmental onset of ooplasmic streaming.

To determine if ooplasmic streaming begins prematurely in *capu* and *spir* oocytes, I examined bulk cytoplasmic movements within living egg chambers. In these experiments, autofluorescent yolk granules within the ooplasm were followed with time-lapse laser scanning confocal microscopy. I displayed the results of these studies as temporal projections, which were generated by the computational summing of consecutive images from confocal time-lapse sequences. In the resulting composite images, stationary granules produced single fluorescent disks, whereas moving granules produced linear arrays of disks (Fig. 2).

In wild-type oocytes from stages 8 through 10a, portions of the ooplasm near the anterior cortex were in constant motion, whereas relatively little movement occurred in more posterior regions (Fig. 2D). The movements within the anterior ooplasm are not coordinated; granules in one subregion may move toward the anterior pole, whereas nearby granules may move toward the posterior pole (*17*). In addition, regions of cytoplasm generally flow along a given trajectory for only a short distance before changing direction (*17*). This "ooplasmic seething" is very different from the coordinated and unidirectional streaming observed in wild-type oocytes from stages 10b through 12 (Fig. 2E). During these stages, most of the ooplasm spins in a uniform direction within the confines of the cortex. These coordinated movements produce spiral patterns in the temporal projections (Fig. 2E). Only a narrow region of ooplasm immediately adjacent to the cortex remains stationary during these stages (Fig. 2E) (*15*).

In both *capu* and *spir* mutant ovaries, time-lapse confocal analyses revealed unidirectional and coordinated ooplasmic movements as soon as yolk granules were detectable, early in stage 8 (Fig. 2, A through C). Ooplasmic streaming continues through stage 12 and terminates during stage 13 (*17*). Time-lapse analyses of earlier egg chambers with the use of differential interference contrast microscopy reveal coordinated organelle movements within the oocyte as early as stage 7 (*17*). Qualitatively similar premature ooplasmic streaming was observed with the two alleles of *capu* and the two alleles of *spir* that were tested (*18*).

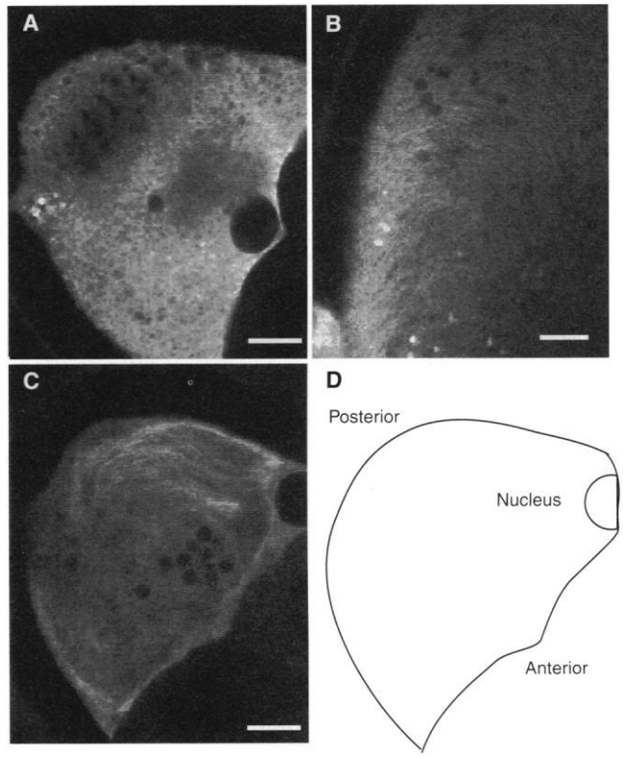

Fig. 1. Microtubule organization in living oocytes. Egg chambers were dissected from wild-type or homozygous mutant females, injected with rhodamine-conjugated tubulin, and examined with a laser scanning confocal microscope (*19*). (**A**) Microtubules in a wild-type stage 8 oocyte. Microtubule concentration was highest at the anterior cortex, and a dense mesh of microtubules extended into the oocyte. (**B**) Microtubule organization during ooplasmic streaming in a wild-type stage 10b oocyte. Parallel arrays of subcortical microtubules were observed. Ooplasmic streaming appears to be driven by organelle movement along these subcortical microtubules. (**C**) Subcortical microtubule arrays in a stage 8 $capu^{G7}/capu^{G7}$ mutant oocyte. These subcortical microtubules are similar to those observed in wild-type oocytes from stages 10b through 12 (B). Subcortical microtubules are also present in stage 8 through 10a *spir/spir* oocytes (*17*). (**D**) Diagram of the stage 8 oocyte shown in (C). Bars are 10 μm.

There are similarities between the premature ooplasmic streaming in *capu* and *spir* oocytes and the streaming in wild-type egg chambers during stages 10b through 12. In both mutant and wild-type oocytes, the most rapid movements occur near the cortical microtubule layer, and the rate of granule movement decreases toward the center of the cell. The maximum rate of streaming in both mutant and wild-type oocytes is also similar and varies between 20 and 25 μm/min (Fig. 2, A through C) (*16*). In addition, streaming in both wild-type and mutant oocytes is blocked by the microtubule-depolymerizing drug Colcemid and is reactivated by 360-nm light, which induces Colcemid photo-isomerization to an inactive form (*17*). The ooplasmic streaming in mutant oocytes from stages 10b through 12 and the termination of streaming in stage 13 mutants are very similar to the same processes in wild-type ovaries (*17*). Thus, *capu* and *spir* do not affect the progress of ooplasmic streaming or the normal termination of this process. These observations indicate that *capu* and *spir* are heterochronic mutations affecting the developmental onset of microtubule-dependent ooplasmic streaming.

The *capu* and *spir* gene products might affect the developmental timing of ooplasmic streaming in several ways. These genes could encode regulatory factors that actively repress ooplasmic streaming until stage 10b. Such factors could form complexes with and inhibit a microtubule motor required for streaming. However, the properties of ooplasmic movement in wild-type oocytes suggest an alternative explanation. The cytoplasmic movements that characterize stages 8 through 10a in wild-type oocytes are not coordinated, and cytoplasmic flow frequently reverses direction. These apparently random movements are inhibited by Colcemid (*17*), which suggests that they are microtubule-dependent. These movements may therefore result from the action of competing plus end– and minus end–directed microtubule-based transport systems. In contrast, the coordinated cytoplasmic movements that characterize stages 10b through 12 appear to be driven by unidirectional microtubule-based transport. Thus, ooplasmic streaming could be initiated by the selective inactivation of one of the competing microtubule-dependent transport systems that function during stages 8 through 10a. In this model, *capu* and *spir* encode components of the transport system that is inactivated as ooplasmic streaming begins. Because only a single transport system is present during the early stages of oogenesis, ooplasmic streaming begins prematurely in the mutant ovaries.

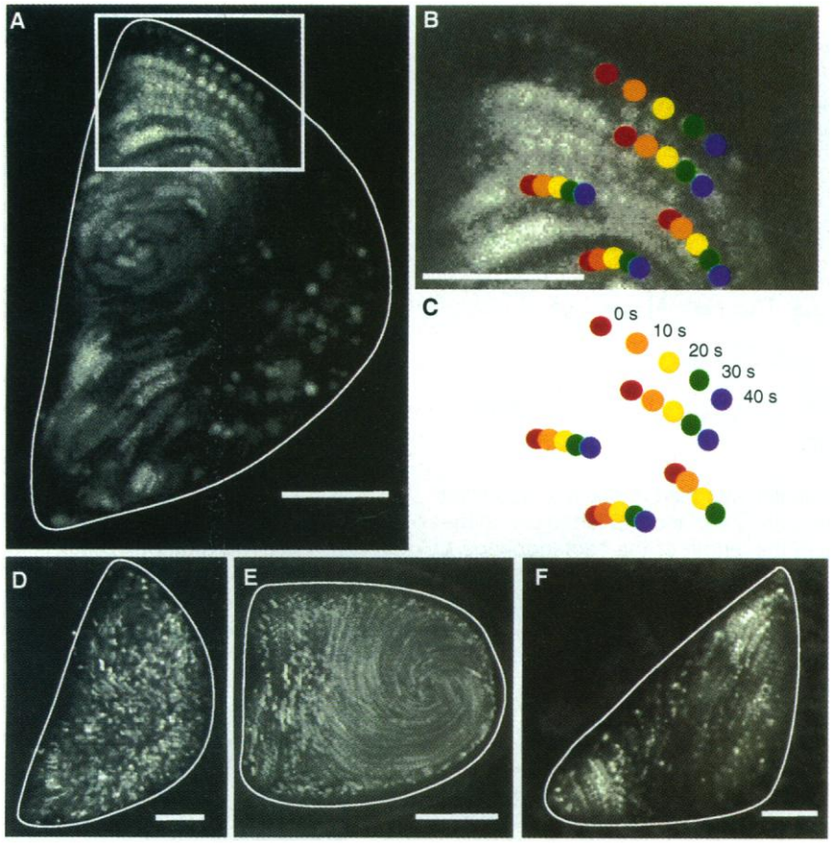

Fig. 2. Premature ooplasmic streaming in *capu* and *spir* mutant oocytes. To detect the movement of bulk ooplasm in living egg chambers, I examined autofluorescent yolk granules with time-lapse laser scanning confocal microscopy (*20*). Temporal projections, showing 100 s of elapsed time, were then constructed by summing 10 images obtained at 10-s intervals. Yolk granules appear as fluorescent disks in these composite images, and granule movements produced linear arrays of disks. (**A**) Ooplasmic streaming within a stage 8 $capu^{G7}/capu^{G7}$ oocyte. Circular cytoplasmic streaming produces a spiral pattern in this projection. (**B**) Details of the boxed portion of the image shown in (A). The positions of five different yolk granules at various times are indicated by color-coded dots. (**C**) Time points represented by the color coding in (B). The initial positions of the granules are indicated by the red dots; the positions at 10 s are in orange, 20 s in yellow, 30 s in green, and 40 s in blue. Note that the most rapid movements, reflected in granule spacing, occur near the oocyte periphery, which is the location of the subcortical microtubule arrays. (**D**) Cytoplasmic movements in a wild-type stage 8 oocyte. Limited, uncoordinated movements were observed near the anterior cortex. (**E**) Ooplasmic streaming in a wild-type stage 10b oocyte. Coordinated cytoplasmic movements produce a spiral pattern in the temporal projection. (**F**) Premature ooplasmic streaming in a stage 9 $spir^{HP10}/spir^{HP10}$ oocyte. In (A), (D), (E), and (F), the oocyte is outlined in white. The bars in panels (A), (B), (D), and (F) are 20 μm. The bar in (E) is 50 μm.

These observations suggest at least two possible causes for the axis specification defects associated with *capu* and *spir*: (i) The premature cytoplasmic movements in mutant oocytes could mechanically disrupt the subcellular localization of morphogenetic molecules or (ii) the changes in microtubule organization that accompany the premature initiation of ooplasmic streaming could be incompatible with the role of these microtubules in axial patterning. The second possibility is consistent with inhibitor studies that indicate microtubules are required for the posterior localization of the protein encoded by *staufen* and *oskar* mRNA (*14*). It is also possible that a combination of these two factors influences the patterning of *capu* and *spir* oocytes. For example, changes in microtubule organization could be the primary cause of the posterior defects associated with *capu* and *spir*, whereas mechanical disruption of morphogen localization may be responsible for the dorsoventral patterning defects. All alleles of *capu* and *spir* produce consistent posterior defects but have variable effects on dorsoventral axis specification (*16*). The differential effects of these mutations on posterior and dorsoventral patterning could reflect distinct underlying mechanisms by which they influence these two axis specification processes.

These observations indicate that the appropriate temporal regulation of ooplasmic streaming is essential to oocyte development. During stages 8 through 10a, the subcellular localization of morphogenetic molecules within the oocyte produces a functionally asymmetric cortex. Ooplasmic streaming during stages 10b through 12, in contrast, mixes newly deposited nurse cell cytoplasm with the existing ooplasm and ensures a homogeneous egg cytosol. The normal temporal regulation of ooplasmic streaming thus allows the establishment of the asymmetry that will direct embryonic differentiation and produces the uniform cytoplasm required to support the rapid and synchronous mitotic divisions that will form the precursors of the embryonic germ line and somatic cells.

REFERENCES AND NOTES

1. C. Nüsslein-Volhard and S. Roth, *CIBA Found. Symp.* **144**, 37 (1989).
2. W. Driever, in *The Development of* Drosophila melanogaster, M. Bate and A. Martinez Arias, Eds. (Cold Spring Harbor Laboratory Press, Cold Spring Harbor, NY, 1993), pp. 301–324.
3. D. St. Johnston, in (*2*), pp. 325–364.
4. D. St. Johnston and C. Nüsslein-Volhard, *Cell* **68**, 201 (1992).
5. A. C. Spradling, in (*2*), pp. 1–70.
6. T. Berleth *et al.*, *EMBO J.* **7**, 1749 (1988).
7. P. F. Lasko and M. Ashburner, *Genes Dev.* **4**, 905 (1990).
8. B. Hay, L. Jan, Y. Jan, *Development* **109**, 425 (1990).
9. J. Kim-Ha, J. Smith, P. MacDonald, *Cell* **66**, 23 (1991).
10. F. S. Neuman-Silberberg and T. Schüpbach, *ibid.* **75**, 165 (1993).
11. E. Koch and R. Spitzer, *Cell Tissue Res.* **228**, 21 (1983).
12. N. J. Pokrywka and E. C. Stephenson, *Development* **113**, 55 (1991).
13. E. Clark, E. Gineger, H. Ruohola-Baker, L. Y. Jan, Y. N. Jan, *Curr. Biol.* **4**, 289 (1994).
14. W. E. Theurkauf, S. Smiley, M. Wong, B. Alberts, *Development* **115**, 923 (1992).
15. H. O. Gutzeit and R. Koppa, *J. Embryol. Exp. Morphol.* **67**, 101 (1982).
16. L. J. Manseau and T. Schüpbach, *Genes Dev.* **3**, 1437 (1989); T. Schüpbach and E. Wieschaus, *Genetics* **129**, 1119 (1991).
17. W. E. Theurkauf, unpublished observations.
18. Ooplasmic streaming was assayed in oocytes homozygous for the following alleles: $capu^{G7}$, $capu^{RK}$, $spir^{PJ56}$, and $spir^{HP10}$. Qualitatively similar premature streaming was observed in all cases. In oocytes isolated from heterozygous mutant females, or in oocytes derived from females homozygous for the *cn*, *bw* second chromosome that was used in the isolation of the *capu* and *spir* alleles (*16*), coordinated ooplasmic streaming was not observed until stage 10b.
19. Microtubules within living oocytes were visualized as follows: 3- to 6-day-old adult females were transferred to a cover glass and covered with halocarbon oil. Egg chambers were removed under oil and were trapped between the cover glass and the oil. The cover glass was then transferred to the stage of an inverted microscope, and the egg chambers were microinjected with rhodamine-conjugated tubulin. Microtubules within the oocytes were visualized with a Bio-Rad MRC 600 laser scanning confocal attachment and a Nikon Diaphot inverted microscope.

20. Bulk ooplasmic movements within living oocytes were assayed as follows: Adult females were transferred to a cover glass and covered with halocarbon oil, and egg chambers were removed and dissected as described (*19*). The cover glass was then transferred to the confocal microscope, and autofluorescent yolk granules were directly imaged with the BHS filter set provided with the Bio-Rad MRC 600 laser scanning confocal microscope. Single frame images were collected at 10-s intervals with the use of the confocal microscope with fluorescein filters. Temporal projections were created by summing 10 frames from a time-lapse sequence with the Project (maximum) utility of the COMOS software provided with the Bio-Rad 600 confocal microscope. Each projection represents 100 s of total elapsed time.
21. Thanks to T. Schüpbach for supplying *capu* and *spir* stocks and to P. Gergen, N. Dean, C. Polk, and the anonymous reviewers for helpful comments on the manuscript. Special thanks to L. Manseau for numerous lively discussions of these results.

22 June 1994; accepted 19 August 1994

Alignment and Sensitive Detection of DNA by a Moving Interface

A. Bensimon,* A. Simon, A. Chiffaudel, V. Croquette, F. Heslot, D. Bensimon

In a process called "molecular combing," DNA molecules attached at one end to a solid surface were extended and aligned by a receding air-water interface and left to dry on the surface. Molecular combing was observed to extend the length of the bacteriophage λ DNA molecule to 21.5 ± 0.5 micrometers (unextended length, 16.2 micrometers). With the combing process, it was possible to (i) extend a chromosomal *Escherichia coli* DNA fragment (10^6 base pairs) and (ii) detect a minute quantity of DNA (10^3 molecules). These results open the way for a faster physical mapping of the genome and for the detection of small quantities of target DNA from a population of molecules.

Extension and manipulation of individual biopolymers is generally performed by first anchoring one end of the molecule at a solid matrix; stretching may then be achieved by viscous drag (*1*, *2*), electrophoresis (*3*), or optical forces (*4*). The method proposed here, which we call "molecular combing," extends a DNA molecule with a receding interface and fixes the molecule in this state on the dry substrate. This physical process leads to a complete, controlled, and reproducible alignment of all DNA fragments, thus allowing accurate position determinations along the molecule.

To anchor DNA to a glass surface, we first grafted a monolayer of silane molecules onto a glass cover slip by methods of "molecular self-assembly" (*5*), exposing a vinyl end group ($-CH=CH_2$) (*6*). These surfaces have the following characteristics: (i) a high binding specificity only for the ends of a DNA molecule—presumably because of the presence of a free protonated phosphate at the 5′ end—with a strong pH dependence, suggesting that the reaction between the molecules and the surface could be a case of electrophilic addition of weak acids to alkenes; (ii) the capability to bind proteins either directly or after oxidation to carboxylic acid groups; and (iii) a strong signal-to-noise ratio resulting from the negligible background fluorescence of glass. However, as usual with silanization procedures (*7*), the quality of the surface treatment is variable. As a result, the percentages of anchored DNA molecules and of their extension vary from batch to batch.

A drop of DNA solution (typically 5 μl) was deposited on a silanated cover slip. An untreated cover slip was then floated on top, forcing the drop to spread to a final thickness of ~20 μm. With video-enhanced fluorescence microscopy, molecules were observed (*8*) not only to be attached at one or both ends (*9*), as deduced from their extension by a flow or by electrophoresis, but also to fluctuate freely in solution (Fig. 1A), thereby indicating the absence of adhering nonspecific interactions between the surface and the molecule.

During evaporation of the DNA solution, the receding air-water interface left the bound molecules fully extended behind and deposited on the dried surface, whereas unbound molecules were swept by the moving interface. The temporal extension of a single fragment of *Escherichia coli* DNA molecule by a receding interface is shown in Fig. 1, B through D, and can lead to the alignment of a molecule 420 μm long (*10*), such as the one shown in Fig. 1E. "Molecular combing" seems to be an irreversible process: upon rehydration, combed molecules remain bound to the surface.

It turns out that the force the interface exerts on the DNA is strong enough to extend it but too weak to break the bond between the molecule and the surface. An estimate of the surface tension force on a rod of diameter D perpendicular to the surface of the interface is $F = \gamma\pi D$, where the surface tension $\gamma = 7 \times 10^{-2}$ N/m for the air-water interface. Because $D = 2.2$ nm for the DNA diameter, $F \approx 4 \times 10^{-10}$ N. This force is two orders of magnitude greater than the entropic forces keeping the DNA molecule in a random coil configuration (*2*) and is thus enough to fully extend the molecule, but it is apparently smaller than the force required to break a covalent bond (on the order of 10^{-9} N) (*11*). Details of the physics of the combing process will be presented elsewhere (*12*).

In contrast to viscous drag and electro-

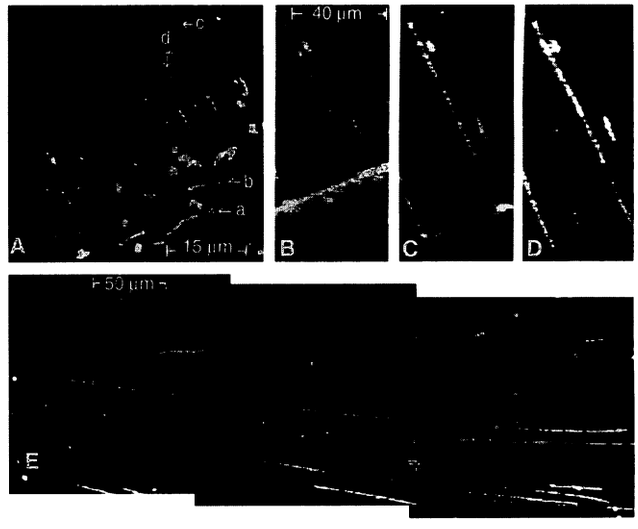

Fig. 1. Extension of DNA by a receding interface. (**A**) Video image showing λ DNA in solution (lower right part of image), bound at one (a) or both extremities (b). The interface extends across the image from the lower left to the upper right. The extended molecules left behind the interface are visible as straight segments (c), if bound at one end, or loops (d), if bound at both ends. (**B** through **D**) Time series showing the extension of a chromosomal *E. coli* DNA fragment by a receding interface (lower part of the image). The time between each pair of video images was 8.5 s. (**E**) Extension of an estimated 10^6–base pair fragment of chromosomal *E. coli*, reassembled from three video images (total length = 420 μm).

A. Bensimon, Neurobiologie Moléculaire, Institut Pasteur, 75015 Paris, France.
A. Simon, A. Chiffaudel, V. Croquette, D. Bensimon, Laboratoire de Physique Statistique, Ecole Normale Supérieure (ENS), 75005 Paris, France.
F. Heslot, Laboratoire de Physique de la Matière Condensée, ENS, 75005 Paris, France.
*To whom correspondence should be addressed.